Application of the rigorous method to x-ray and neutron beam scattering on rough surfaces

Leonid I. Goray[a)]
Saint Petersburg Academic University, Khlopina 8/3, St. Petersburg 194021, Russian Federation; Institute for Analytical Instrumentation, RAS, Rizhsky Prospect 26, St. Petersburg 190103, Russian Federation; and I.I.G., Inc., P.O. Box 131611, Staten Island, New York 10313, USA

(Received 22 March 2010; accepted 30 June 2010; published online 6 August 2010)

The paper presents a comprehensive numerical analysis of x-ray and neutron scattering from finite-conducting rough surfaces which is performed in the frame of the boundary integral equation method in a rigorous formulation for high ratios of characteristic dimension to wavelength. The single integral equation obtained involves boundary integrals of the single and double layer potentials. A more general treatment of the energy conservation law applicable to absorption gratings and rough mirrors is considered. In order to compute the scattering intensity of rough surfaces using the forward electromagnetic solver, Monte Carlo simulation is employed to average the deterministic diffraction grating efficiency due to individual surfaces over an ensemble of realizations. Some rules appropriate for numerical implementation of the theory at small wavelength-to-period ratios are presented. The difference between the rigorous approach and approximations can be clearly seen in specular reflectances of Au mirrors with different roughness parameters at wavelengths where grazing incidence occurs at close to or larger than the critical angle. This difference may give rise to wrong estimates of rms roughness and correlation length if they are obtained by comparing experimental data with calculations. Besides, the rigorous approach permits taking into account any known roughness statistics and allows exact computation of diffuse scattering. © *2010 American Institute of Physics*. [doi:10.1063/1.3467937]

I. INTRODUCTION

Multiwave and multiple diffraction, refraction, absorption, waveguiding, and wave deformation govern to a considerable extent scattering of x-ray and extreme ultraviolet (EUV) radiation and cold neutrons from nanoroughness of continuous media. Inclusion of these pure dynamic effects, which requires application of electromagnetic theory, permits one to calculate the absolute intensity of the specular component and describe adequately the intensity distribution of the diffuse component which may have resonance peaks. Besides, there are cases in which the vector character of x-rays cannot be ignored.[1,2] Some surfaces are deterministic (e.g., perfect gratings) and some are random (e.g., polished mirrors). Some surfaces are one-dimensional (1D) (e.g., real 1D gratings and cutting mirrors) but most are two-dimensional (2D) (e.g., 2D gratings, ocean surfaces, and surfaces with atomic scale roughness). Any number of possible combinations between these four characteristics may be present in real structures (e.g., machined 1D deterministic surfaces with 2D random roughness). The question of the closeness of results for 1D and 2D surfaces is of interest, since numerical methods for 1D surfaces are well established and efficient, and widely used for surfaces with 2D roughness.[3] Despite the impressive progress reached recently in development of exact numerical methods of investigation of wave diffraction from boundary roughness,[3–6] the present author is aware only of asymptotic and perturbation approaches to the analysis of x-ray and neutron scattering, even from 1D rough surfaces, such as the Kirchhoff approximation, method of parabolic wave equation, Rayleigh method, Born approximation (BA), distorted-wave BA (DWBA), and a few others.[7–9] Note also that method mentioned in Ref. 10 as exact for inclusion of any type roughness and based on the boundary integral equations cannot be considered as valid for x-rays on account of an absence of implementation details and examples in that paper.

The well-known Debye–Waller (DW) asymptotic, which can be derived from the BA, is commonly used in the region where angle of incidence θ measured from the surface normal must be smaller and far from the critical incidence angle. The Nevot–Croce (NC) model, which can be derived from the first-order DWBA, is used mostly at grazing incidence near or below the critical angle. The both factors of the reduction in specular reflectance are valid, strictly speaking, in the case of small rough boundary heights h and very large (DW) or very small (NC) correlation lengths ξ.[8] The second-order DWBA should be used to take into account arbitrary magnitudes of ξ, however it is valid generally for small values of $h \cos\theta/\lambda$, where λ is the vacuum wavelength. Moreover, it was shown[11] and corroborated by the present computations that the rms roughness σ and ξ, which determines the properties of scattering from rough surfaces, become no longer adequate for description of the diffuse intensity pattern after $\sigma \cos\theta$ has exceeded approximately $\lambda/10$. The use of the above or even more sophisticated approximations in cases of the intermediate incident angle range and comparable magnitudes of λ, σ, and ξ also appears very questionable.

[a)]Electronic mail: lig@pcgrate.com.

It is well-known that solution of the 2D Helmholtz equation with any rigorous numerical code meets with difficulties at high ratios of characteristic dimension to wavelength.[12–18] While the known boundary integral equation methods are robust, reliable, and efficient, they exhibit poor convergence and loss of accuracy in the high-frequency range due to numerical contamination in quadratures. Increasing matrix size and enhancing computation precision, as well as application of convergence speed-up techniques, which are successfully explored in low-frequency and mid-frequency ranges, lead to unreasonably stringent requirements for computing times and storage capacities in high-frequency ranges. The rigorous modified method of boundary integral equations (MIM) (Refs. 19–21) has been widely employed in analyzing the efficiency of bulk and multilayered diffraction gratings, including but not restricted[22] to those in the x-ray-EUV range.[23] The approach is very accurate and fairly fast convergent in the range of very small ratios of λ to period d and groove depth h, particularly for structures with real boundary profiles.[24–26] The method, which has been developed in the frame of rigorous theory (i.e., with the use of Maxwell's equations, rigorous boundary conditions and radiation conditions), permits application of optical methods to analysis of specular and nonspecular x-ray scattering from rough mirrors in real space. In the case of one boundary the system of two Helmholtz equations can be reduced to one integral equation which contains boundary integrals of the single and double layer potentials.

For exact account of random roughness, the method makes use of the well-known model (see, e.g., Refs. 27 and 28), in which a randomized surface is identified with a grating with a large d containing a large number of random asperities. Thus, the method analyzes periodical structures, which may be considered as gratings from a pure mathematical standpoint while representing in actual fact a rough surface if d is chosen much larger than the correlation length ξ of the asperities. Furthermore, in cases where ξ is comparable with λ, and the number of orders is large, the continuous angular distribution of diffuse intensity reflected from a random boundary can be described by a discrete angular distribution of grating order efficiency. The author must emphasize that this approach enables one to deal with particular profiles of the deterministic surface roughness to calculate the average scattering intensity using the forward electromagnetic code and Monte Carlo simulation. Provided the sample is large enough, the roughness properties average out but there is no assumption including averaging in this model. The present paper addresses rigorous simulation of grazing-incidence x-ray scattering as applied to finite-conducting 1D surfaces with random roughnesses in the case of beam incidence in the plane perpendicular to the relief (classical 2D diffraction). The boundary integral equations applicable for the three-dimensional (3D) case of conical (off-plane) diffraction is described in detail in Ref. 29. Data obtained by the rigorous approach and approximate methods are found to be noticeably different, however, in the cases of near-normal incidence, arbitrary incident beam orientation, perfect boundary conductivity, multilayer rough mirrors and randomly rough diffraction gratings as well; but these problems have to be considered elsewhere.

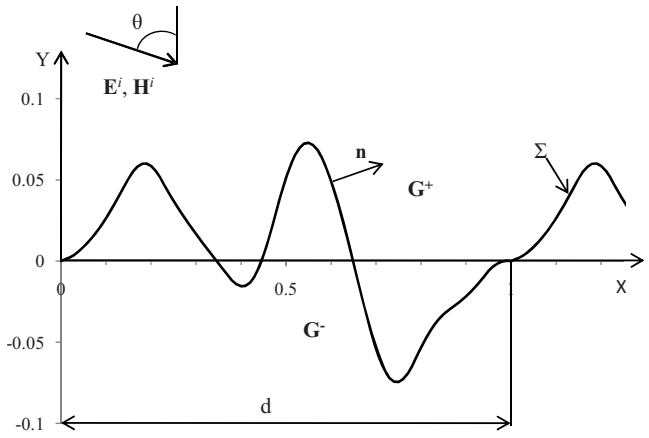

FIG. 1. Schematic cross section of a grating.

The paper is organized as follows. The corresponding theory of the developed MIM is described in Sec. II. The diffraction problem, boundary conditions, and outgoing wave conditions are formulated in Sec. II A. The respective integral equation expressed in terms of boundary potentials can be found in Sec. II B. A more general treatment of the energy conservation law applicable to absorption gratings and rough mirrors is considered in Sec. II C. The peculiarities of the MIM and its numerical implementation expedient for the calculation of $\lambda/d \ll 1$ and $\lambda/h \ll 1$ diffraction problems are described in Sec. III. The discretization details, evaluation of kernels and their summation rule are described in Secs. III A–III C, respectively. A numerical implementation approach and its validation are described briefly in Sec. III D. Finally, in Sec. IV numerical experiments for randomly rough Au mirrors operating with hard and soft x-rays are demonstrated as an illustration of the possibilities inherent in the MIM.

II. THEORY

A. Diffraction problem

The grating is a cylindrical surface whose generatrices are parallel to the z-axis and whose cross section in the (x,y)-plane is given by the simple curve Σ (see Fig. 1). We assume that the open arc Γ denotes one period d in x-direction of Σ. One refers to the nonabsorption top G^+ and generally absorption bottom G^- semi-infinite media. It is assumed that the radiation incident from G^+ in the $Y0X$ plane with the pulsatance ω scales with time as $e^{-i\omega t}$ and that the process is stationary. Because Σ is not varying in the z direction, it is possible to consider the two fundamental cases of polarization separately, i.e., the TE mode (with the z component E_z^i of the electric field $\mathbf{E}^i$ parallel to the grating grooves) and the TM mode (with the z component H_z^i of the magnetic field $\mathbf{H}^i$ parallel to the grating grooves).[18] The wavenumber inside $G^+ \times \mathbb{R}$ is denoted by $k^+=(\alpha,-\beta,0)$. Thus, the original 3D problem reduces to a 2D one and becomes independent of the z direction of the grating

$$u^i(x,y) = E_z^i(x,y)e^{i(\alpha x-\beta y)} \quad (\mathrm{TE,s}),$$

$$u^i(x,y) = H_z^i(x,y)e^{i(\alpha x-\beta y)} \quad (\mathrm{TM,p}), \tag{1}$$

where $\alpha=k^+ \sin\theta$, $\beta=k^+\cos\theta$, and $|\theta|<\pi/2$.

The components of the wave vector $\mathbf{k}^\pm$ for $(x,y)\in G^\pm$ satisfy the conditions $\beta>0$ and $(k^\pm)^2=\omega^2\varepsilon^\pm\mu^\pm=(\omega\nu^\pm)^2$, with piecewise constant functions of electric permittivity and magnetic permeability $\varepsilon(x,y)=\varepsilon^\pm$ and $\mu(x,y)=\mu^\pm$, respectively. Due to the periodicity of Σ, the incident wave is scattered into a finite number of plane waves in $G^+\times\mathbb{R}$. Classical diffraction corresponds to $\mathbf{k}^+\cdot\mathbf{e}_z=0$, whereas $\mathbf{k}^+\cdot\mathbf{e}_z\neq 0$ characterizes conical diffraction.[29]

Maxwell's equations imply that the total fields $E_z=u^\pm$ or $H_z=u^\pm$ satisfy the Helmholtz equation in $G^\pm$

$$(\Delta+(k^\pm)^2)u^\pm=0. \tag{2}$$

The z-components of the incoming field are α-quasiperiodic in x with a period d, i.e., they satisfy the relation

$$u^i(x+d,y)=e^{id\alpha}u^i(x,y). \tag{3}$$

The periodicity ε and μ suggests that one should look for α-quasiperiodic solutions $u^\pm(x,y)$. Furthermore, the diffracted field must remain bounded at infinity, which implies the well-known outgoing wave conditions (the Sommerfeld radiation conditions) represented in the form of the Rayleigh expansion in the far field with complex c_m^+ order amplitudes in the upper (+) and lower (−) mediums

$$u^+(x,y)=u^i+\sum_{m\in\mathbb{Z}}c_m^+e^{i(\alpha_m x+\beta_m^+ y)}, \quad y\geq h/2,$$

$$u^-(x,y)=\sum_{m\in\mathbb{Z}}c_m^-e^{i(\alpha_m x-\beta_m^- y)}, \quad y\leq -h/2, \tag{4}$$

where $\Sigma\subset\{(x,y):|y|<h/2\}$ and α_m, $\beta_m^\pm$ for the order number m are given by relations

$$\alpha_m=\alpha+\frac{2\pi m}{d}, \quad \beta_m^\pm=\sqrt{(k^\pm)^2-\alpha_m^2}, \tag{5}$$

where $0\leq\arg\beta_m^\pm<\pi$.

By invoking the continuity of the tangential components of $\mathbf{E}$ and $\mathbf{H}$ on the surface we can write the jump conditions in the form

$$[u^+]_\Sigma=[u^-]_\Sigma=0,$$

$$[v^+]_\Sigma=q[v^-]_\Sigma, \tag{6}$$

where $[.]$ denotes the jump of functions on Σ, $v^\pm=\partial_n u^\pm$ is the normal derivative $\partial_n=n_x\partial_x+n_y\partial_y$ on Σ, and $q=\mu^-/\mu^+$ or $q=\varepsilon^-/\varepsilon^+$ for the s-component or p-component, respectively.

Denoting the normal derivative of z-components of the incident field by v^i, we see that the problems (1)–(6) is defined completely in respect to $u^\pm$ and $v^\pm$.

B. Integral equations

The boundary integral equation approach of the present paper transforms the problems (1)–(6) into a system of integral equations over the profile curve. To transform the diffraction problem for the quasiperiodic Helmholtz equations in $\mathbb{R}^2$ to integral equations the boundary integral operators have been used. Analytical properties of integral operators, including avoidance of hypersingular operators, are described in many publications (see, e.g., Refs. 30–32). Moreover, the existence and uniqueness of solutions in appropriate function spaces ensure convergence of a numerical method.

We assume here that Σ is a nonself-intersecting profile given by a piecewise C^2 parametrization $\sigma(s)=[X(s),Y(s)]$ with $s\in\mathbb{R}$, which has to fulfil conditions

$$X(0)=0, \ X(L)=d, \ Y(0)=Y(L), \ Y(s+L)=Y(s),$$

$$X(s+L)=X(s)+d, \ Y(s+L)=Y(s), \tag{7}$$

where L is the arc length of the profile Γ, $\sigma(s_1)\neq\sigma(s_2)$ if $s_1\neq s_2$, and

$$|\sigma'(s)|=\sqrt{[X'(s)]^2+[Y'(s)]^2}>0,$$

$$n_X=-Y'(s)/|\sigma'(s)|, \ n_Y=X'(s)/|\sigma'(s)|, \tag{8}$$

where $n_X(P)$ and $n_Y(P)$ are components of the vector $\mathbf{n}(P)$ normal to Γ at $P[X(s),Y(s)]$ and pointing into G^+, and the prime denotes d/ds. If the profile Σ has corners, then we assume additionally that the angles between adjacent tangents at the corners are confined between 0 and 2π.[20] The functions $u^\pm,v^\pm$ are identified by the upper (+) and lower (−) limits of the single and double layer potentials on Γ defined as

$$V_{k^\pm}^\pm w^\pm(P)=\int_\Gamma w^\pm(Q)\Psi_{k^\pm}(P-Q)d\sigma_Q,$$

$$W_{k^\pm}^\pm \tau^\pm(P)=\int_\Gamma \tau^\pm(Q)\partial_{n(Q)}\Psi_{k^\pm}(P-Q)d\sigma_Q, \tag{9}$$

where $w^\pm,\tau^\pm$ are unknown density functions, $P,Q\in\Gamma$, and $\Psi_{k^\pm}(P)$ are the quasiperiodic fundamental solutions (the Green functions) of period d given by the infinite series

$$\Psi_{k^\pm}(P)=\frac{i}{4}\sum_{m=-\infty}^{\infty}H_0^{(1)}[k^\pm\sqrt{(X-md)^2+Y^2}]\times e^{imd\alpha}$$

$$=\frac{i}{2d}\sum_{m=-\infty}^{\infty}\frac{e^{i(\alpha_m X+\beta_m^\pm|Y|)}}{\beta_m^\pm}, \tag{10}$$

where $H_0^{(1)}$ is the first Hankel function of zero order. In Eq. (9), $d\sigma_Q$ denotes integration with respect to the arc length.

The solution is sought in the general form as the sum of the single and double layer potentials[30]

$$u^+=(V_{k^+}w^+)(x,y)+(W_{k^+}\tau^+)(x,y)+u^i(x,y),$$

$$u^-=(V_{k^-}w^-)(x,y)+(W_{k^-}\tau^-)(x,y). \tag{11}$$

With Eq. (11), the conditions (2)–(4) are fulfilled automatically, and the boundary conditions also have to be fulfilled. The single and double layer potentials satisfy the continuity condition for $V_{k^\pm}\varphi$ and the well-known jump relation for $W_{k^\pm}\varphi$ through Γ:

$$(V_{k^\pm}\varphi)^+ = (V_{k^\pm}\varphi)^- = (V_{k^\pm}\varphi),$$

$$(W_{k^\pm}\varphi)^\pm = (W_{k^\pm}\varphi) \pm \varphi/2. \tag{12}$$

Now Eq. (6) read as

$$V_{k^+}w^+ + \tau^+/2 + W_{k^+}\tau^+ + u^i = V_{k^-}w^- - \tau^-/2 + W_{k^-}\tau^-,$$

$$q(U_{k^+}w^+ + w^+/2 + \partial_n W_{k^+}\tau^+ + v^i) = U_{k^-}w^- - w^-/2 + \partial_n W_{k^-}\tau^-, \tag{13}$$

with the additional boundary operator for the normal derivative of the single layer potential defined by

$$U^\pm_{k^\pm}w^\pm(P) = \int_\Gamma w^\pm(Q)\partial_{n(P)}\Psi_{k^\pm}(P-Q)d\sigma_Q. \tag{14}$$

A few degrees of freedom exist for choosing a system of integral equations, and the uniqueness theorem can be applied.[31] For example, the hypersingular operators $\partial_n W_{k^\pm}\tau^\pm$ can be eliminated by an appropriate choice of the unknown functions. Also, single integral equations can be derived from Eqs. (11) and (13).[31] The choice of functions $\tau^+=0$, $\tau^-=-u^+$, and $w^-=-q\partial_n u^+$ leads to the solution of the single integral equation in respect to w^+ (Refs. 18 and 26)

$$[qV_{k^-}(U_{k^+}+I/2) + (W_{k^-}+I/2)V_{k^+}]w^+ = -u^i(W_{k^-}+I/2) - qv^iV_{k^-}. \tag{15}$$

The integral Eq. (15) has been implemented in the code described in the present paper.

C. Efficiency, absorption, and energy balance

Diffraction efficiencies or far field patterns for the reflected fields can easily be found from the corresponding boundary values. In the upper medium the amplitudes for diffraction order number m can be obtained from Eq. (11) and the Rayleigh expansion for the plane waves [see Eq. (4)] by equating coefficients for the corresponding harmonics:

$$c^+_m = \int_\Gamma \mathrm{e}^{-\mathrm{i}[2\pi m X(s)/d + \beta^+_m Y(s)]}w^+(Q)d\sigma_Q/2\mathrm{i}d\beta^+_\mathrm{m}. \tag{16}$$

The efficiency of a diffracted order represents the fraction of power radiated in each order. Defining the power as the flux of the Pointing vector modulus $|\mathbf{S}^i| = 0.5\ \mathrm{Re}\ \mathbf{E}^i \times \overline{\mathbf{H}^i}$ ($\bar{O}$ denotes the complex conjugate of O) through a normalized rectangle parallel to the (x,z)-plane, the ratio of the power of a reflected propagating order and of the incident wave gives the diffraction efficiency η^+_m of this order. For the partially polarized incident light with the s-component and the p-component the efficiency can be found as

$$\eta^+_m = (|c^{+s}_m|^2 \sin^2\delta + |c^{+p}_m|^2\cos^2\delta)\beta^+_m/\beta, \tag{17}$$

where incident and diffracted plane waves are given by the polarization angle $\delta = \arctan(|E^i_z|/|H^i_z|)$ with the normalization $|E^i_z|^2 + |H^i_z|^2 = 1$.

For $\lambda/d \ll 1$ the discrete order efficiencies is an approximation of the differential scattering intensity (bistatic scattering coefficient[33]) for a continuum of scattered angles

$$\zeta(\theta_m) = d\cos^2(\theta_m)|c^{+s,p}_m|^2/\lambda, \tag{18}$$

where $\cos(\theta_m) = \beta^+_m/k^+$ and

$$\sum_{\beta^+_m>0}\eta^+_m = \int_{-\pi/2}^{\pi/2}\zeta(\theta_m)d\theta_m. \tag{19}$$

One of the most important accuracy criteria based on a single computation is the energy balance that can be generalized in the lossy case described below. If the grating is absorbing, $\mathrm{Im}\ \nu^- \neq 0$, then conservation of energy is expressed by a criterion

$$R + A = \sum_{\beta^+_m>0}\eta^+_m + A = 1, \tag{20}$$

where R is the sum of the reflection order efficiencies and A is called the absorption coefficient or simply the absorption in the given diffraction problem. Besides being physically meaningful, expression (20) is very useful as one of numerical accuracy tests for computational codes and especially important in the x-ray and EUV ranges, where absorption plays a predominant role. In the lossy case, one needs an independently calculated quantity A to verify Eq. (20). For such a quantity, we use the absorption integral introduced in Ref. 22 and derived in Appendix. The sum $R+A$ is actually the energy balance for an absorbing grating or a rough mirror, and the extent to which it approaches unity is a measure of the accuracy of a calculation.

III. PECULIARITIES OF MIM AND ITS NUMERICAL IMPLEMENTATION

The boundary integral equation theory is so flexible that we can point out a few areas of its modifiability.[20] (1) In the physical model one can choose boundary types (periodical or nonperiodical, closed or nonclosed, smooth or having edges, randomly rough or deterministic, etc.) and boundary conditions (rigorous or nonrigorous, perfect or finite conducting, etc.). (2) In the mathematical structure, integral representations using various potential operators and/or integral formulas can be considered. (3) In the method of discretization, trial functions (piecewise constant, or trigonometric, or spline, or delta, etc.) and numerical scheme of discretization including treatment of corners in boundary profile curves (Galerkin, or collocation, or Nyström collocation, hybrid, etc.) can be chosen. (4) In the low-level details one can define methods of calculations of kernels (direct methods using Hankel or exponential functions, or Ewald's method, or high-order summations, etc.; and using or nonusing acceleration techniques like as Kummer or Euler–Knopp summation, or single-term corrections, etc.), meshes of sampling (collocation) points (uniform or nonuniform), quadrature rules (trapezium or more sophisticated), solutions of linear systems (direct methods or iterative solvers), caching of repeating quantities (exponential functions, kernel functions, etc.). A self-consistent explanation of various integral methods is well beyond the scope of this study, and one should rather be addressed to references. In this section, special attention is

paid to important aspects of the presented MIM for small λ/d diffraction problems in connection with (3) and (4), and also, briefly, numerical implementations.

A. Discretization details

In practice, the convergence and accuracy of efficiency computation significantly depend on a proper choice of trial functions, discretization schemes, and respective quadrature rules. Usually, one of collocation methods (method of moments) is used with the distribution of points on a uniform grid.[12] To transform the diffraction problem for the Helmholtz equations in $\mathbb{R}^2$ to the single integral equation using the boundary integral operators the combination of direct and indirect approaches is applied here as classified in Refs. 18 and 31. In the MIM, the fastest Nyström discretization with piecewise constant trial functions is used (cf. Ref. 22), where the integrals in the integral operators are approximated by the quadrature rule with the collocation points used as quadrature knots. Such fully discrete method combined with the simplest rectangle (trapezium) integration rule works well for shallow border profile gratings and, especially, at small λ/d.[19,23,26]

A possible function of the distance between collocation points can be prescribed by equal steps along the axis perpendicular to the grooves.[20] As pointed out in Ref. 18 and what is valid for x-rays, in the case of regular kernels and periodic integrand functions, a step function approximation of the integrand expression, with division of the integration interval (period) into equal parts, is preferable. In the presence of a profile with corners (piecewise linear), the collocation and quadrature nodes are set in such a way that every corner lies half-way between the nodes adjacent to it and no curvature-like single-term corrections are added to Green's function normal derivatives.[21] However, for deep groove calculations another version of the quadrature formula involving the normal derivative of the Green's functions can be used. The nodes are set in such a way that all corners are nodes and the curvature corrections are applied by adding the corner term.[20] For such diffraction structures better results are often obtained using equidistant integration steps along the arc length.[13,15,21] A more efficient approach with meshes of collocation points graded toward the corner points of the profile curves together with the appropriated quadrature rule is introduced in Ref. 12.

B. Evaluation of kernels

In spite of many research efforts (see, e.g., Refs. 34 and 35) and power of modern computers, computation of the kernel functions remains a time- and accuracy-critical part of integral methods for periodic structures, and especially for $\lambda/d \ll 1$. To accelerate convergence of the series representing kernels, different acceleration techniques are applied (cf., e.g., Ref. 12). In the present approach, the peculiarity discovered in Ref. 36 and described in Ref. 20 is used in the case of shallow gratings and rough mirrors working at very small λ/d: "Introducing known speed-up terms in integral methods produces an adverse numerical effect because of the ensuing uncontrolled growth of coefficients in analytically improved asymptotic estimations." As shown further with all speed-up options turned off, it is possible to obtain for the most difficult problems surprisingly rapid convergence, and an energy balance very close to 1.

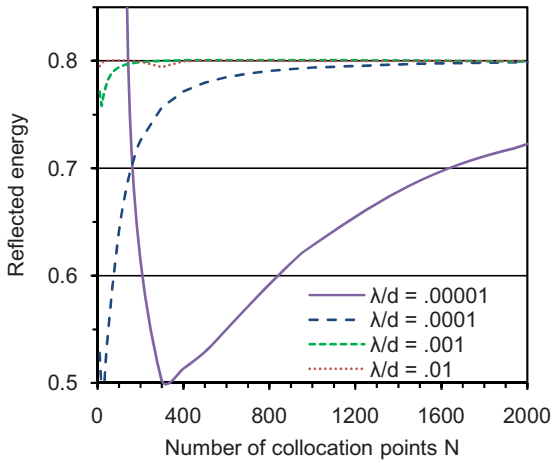

FIG. 2. (Color online) Reflected energy obtained by the MIM with speed-up techniques for the problem of diffraction on a perfect Au interface of radiation with $\lambda=1$ nm incident at $\theta=89°$ plotted vs N for different λ/d.

In Fig. 2, convergence of the present integral method is demonstrated in respect to the main cut-off parameter N for an analytically amenable case of x-ray diffraction from a plane absorbing interface (grazing incidence in vacuum of nonpolarized radiation to perfect Au surface prescribed by a zero-depth sinusoidal profile) for $\lambda=1$ nm, $\theta=89°$, and different λ/d. The refractive indices of Au for all examples were taken from Ref. 37. For $\lambda/d=1.E-2$, the convergence rate reached using speed-up techniques is high, with the reflected energy error of $\sim 4.9E-6$ for the number of collocation points $N=40$ (the exact reflectance value is 0.7999). For $\lambda/d=1.E-3$, the convergence rate reached with speed-up techniques is medium, with the reflected energy error of $\sim 1.E-3$ for $N=200$. For $\lambda/d=1.E-4$, the convergence rate, again obtained with speed-up techniques, is low with the reflected energy error of $\sim 6.2E-3$ for $N=1000$. For $\lambda/d=1.E-5$, the convergence rate calculated with speed-up techniques is very low, with the reflected energy error of $\sim 7.7E-2$ for $N=2000$. In contrast to the plots of Fig. 2, the results for extremely low λ/d of $1.E-7$ obtained without application of any speed-up techniques exhibit the fastest convergence rate with a negligible reflected energy error of $\sim 1.E-16$ for $N=2$ only and are equivalent to analytical calculations. The most important among the convergence speed-up options which have to be switched off in this case is the allowance for logarithmic singularity, and second important, is the correction applied to account for the cut-off terms in the expansions of kernels (the Aitken's δ^2 single-term correction in our case).[38] Switching off the curvature single-term correction is of a lower but not minor significance on the way to reaching fast convergence. While the results presented in Fig. 2 may certainly be different for various realizations of integral methods and of speed-up techniques used, the overall pattern remains the same. Such calculations depend also significantly, as shown in Fig. 3 and will be discussed further, on the actual summation rule chosen for kernels.

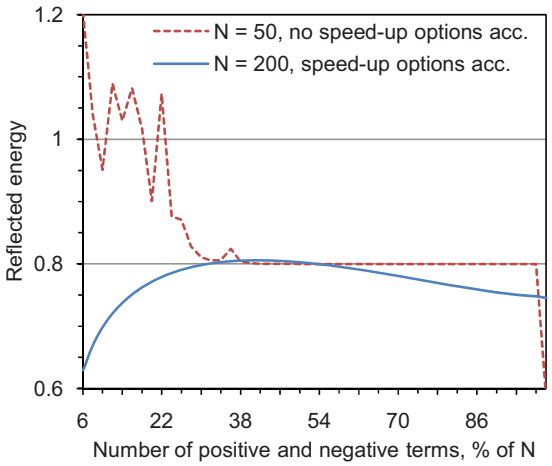

FIG. 3. (Color online) Reflected energy obtained by the MIM for the same problem as in Fig. 2 and for $\lambda/d=0.001$ vs g for different N and with or without allowance for speed-up techniques.

Shallow gratings with real (polygonal) groove profiles and rough mirrors exhibit a very similar behavior for very low λ/d in x-ray–EUV. While at least one collocation point per wavelength is required to reach efficiency convergence for the usual integral methods, the MIM works reliably and fast despite the very small number of collocation points per wavelength used in the approach (it is also true for echelles).[13,15,20] For example, if a period includes 100 collocation points and $\lambda/d=1.E-5$, there is only $1.E-3$ point per wavelength required for the MIM. In this case, however, the profile depth and the incident radiation wavelength should be of the same order of magnitude. The same rule for reaching the maximum diffraction efficiency is, on the whole, valid for longer wavelengths too.

C. Summation rule for kernel functions

The MIM described here specifies the number of positive and negative terms in Green's functions and their normal derivative expansions. In the simplest case typical of real problems, the series are truncated symmetrically at the lower summation index $-P$ and the upper index $+P$, where P is an integer defined by

$$P \approx gN. \tag{21}$$

The truncation ratio g is optimized for small values of N and is kept constant as N increases. It was found that P equal to 50% of N is a reasonably good choice for most practical computations and, in particular, for small λ/d. The typical dependence on P for the above example with $\lambda/d=1.E-3$ is shown in Fig. 3. For calculations with $N=200$ and speed-up techniques the reflected energy is close to the exact value with the error of $2.E-5$ at $g=1/2$, with some divergence seen to set in at smaller and larger values of g. For calculations with $N=50$ without applying speed-up techniques the reflected energy is equal to the exact value, again, at $P=0.5N$, with some divergence seen to set in with smaller number of terms.

While today this rule is no more than empirical, there can be no doubt whatsoever that this choice is valid, and this has been verified in many realistic examples during the recent years. Note that in the integral method developed in Ref. 18, $g=2/3$ for the resonance domain and should be varied for different λ/d. It is worth noting that $g=2/3$ is worse than $g=1/2$ because the computation time is proportional to $2PN^2$. Significantly, P used in computations of kernels should be restricted to be not larger than N, because such series diverge for $P \geq N$ (see Fig. 3 at a point $P=N$).[18,21,22]

Instead of the direct summation algorithm used in the MIM, more sophisticated methods can be implemented to accelerate the computation of integral kernels (cf., e.g., Ref. 29). Unfortunately, it has turned out that such approaches are not efficient for very small λ/d.

One more important note regarding the energy balance summation appears to be pertinent here. Kernels functions tend to to become large when the y-component $\beta_m^{\pm}$ of the mth diffraction order wave vector in the upper medium or/and in the lower medium (for transmission gratings) tends to zero. This means that the diffraction order becomes grazing or even close to evanescent. Its efficiency may be high from the physical point of view or/and diverge from the mathematical point of view (it depends also on N). It is well known from diffraction theory that the efficiency of strictly grazing propagating, as well as of all evanescent, orders is zero. Moreover, various rigorous and approximate methods valid for shallow gratings operating at small λ/d, as well as all experimental data suggest convincingly that the efficiency decreases rapidly with increasing modulus of the diffraction order number. As a rule, the efficiencies of such grazing orders are very close to zero and much less than the error of computations. Thus, such big efficiency values which correspond to high grazing orders must be excluded from the energy balance consideration.

D. Numerical implementation and validation

To reduce computing time for matrices of the discretized operator equations, two enhancements at the algorithmic level are used in the MIM: cache for the kernel functions and cache for exponential functions (plane waves). Both assume a big time-memory trade-off at small λ/d. The amount of memory required for cache can be calculated in advance in each case and adjustments (cache off or partial) are done automatically. One can find the details of the cache implementation in Ref. 22.

To study the scattering intensity using a forward electromagnetic code and Monte Carlo simulation, one should first of all generate statistical realizations of the boundary profiles of the structure under investigation, then calculate the scattering intensity for each realization and, finally, average the intensities over all the realizations. The present author used a spectral method[33] to generate plane surfaces with a Gaussian height distribution and a Gaussian correlation function with the Hurst parameter $H=1$.[39] To allow randomization of grating boundaries, this method was extended to include the case of nonplane interfaces prescribed by arbitrary polygons.[40] Nonplane boundaries are characteristic also of self-

assembled low-dimensional quantum structures [e.g., quantum dots (QDs), quantum molecules, and whiskers] defined by other asperity statistics.[41]

A few words regarding the extent to which the calculations made in extremely hard cases can be trusted are in order here. The workability of the program has been confirmed by numerous tests usually employed in nonextreme cases, more specifically, the reciprocity theorem, stabilization of results under doubling of N and variation in g, comparison with analytically amenable cases of plane interfaces, consideration of the inverse (nonphysical) radiation condition, use of different variants of collocation point distribution and shifts, comparison with the results obtained by other available codes or with published data, or with information corresponded to the author by other researchers, including results of measurements.

IV. SPECULAR X-RAY REFLECTANCES OF ROUGH SURFACES

In this section, we are going to address the results of numerical study of grazing-incidence specular reflection of hard and soft x-rays from typical gold randomly rough mirrors with Gaussian roughness statistics. Readers interested in grazing-incidence x-ray reflectometry of multilayer randomly rough gratings and single- and multilayer quasiperiodical ensembles of In(Ga)As/GaAs and Ge/Si QDs performed in the frame of the MIM including nonspecular scattering are referred to Refs. 41–44.

A vacuum-Au surface model with the Gaussian roughness height distribution and Gaussian correlation function for use at grazing incidence near the angle of total external reflection was chosen as an example. The difference between the rigorous and asymptotic approaches can be clearly seen in the figures which plot the calculated specular TE reflectances (TM reflectance data are close in magnitude) of Au surfaces vs. the angle of incidence for different values of rms roughness σ, correlation length ξ, and λ. For the BA (DW corrections),[45,46] $\xi=\infty$, for the first-order DWBA (Ref. 39) (NC corrections),[45] $\xi=0$, and for the rigorous model, chosen ξ are close to the asymptotic values or have intermediate values.

A comparison between the rigorous and approximate models for Cu $K_{\alpha 1}$ radiation ($\lambda=0.154$ nm), $\xi=5$ nm (the rigorous model) and different σ is shown in Figs. 4 and 5. For $\sigma=0.15$ nm (Fig. 4), the results obtained for all the models differ only by a few % within the angular range studied. For $\sigma=1.5$ nm in Fig. 5, the difference is about an order of magnitude in the low reflectance range, and about a few times in the intermediate range. Close to the critical angle, this excess amounts to ~10% compared with the figure derived from the DWBA. Such pronounced differences may bring about an overestimation of σ if it is deduced from a comparison of experimental data with calculations.[45] Significantly, only 10–15 random asperities within d and about as many statistical realizations turned out to be sufficient for the average values of the reflectance in the examples of Figs. 4 and 5 to converge. N required to reach convergence and the desired accuracy ($\sim 1.E-5$) as estimated from the energy balance was found to be 2000.[41] Note that in the deep roughness case, the convergence speed-up techniques were used. The time taken up by one rigorous computation on a workstation with two Quad-Core Intel® Xeon® 2.66 GHz processors, 8 MB L2 Cache, 1333 MHz FSB, and 16 GB RAM, is ~16 min when operating on Windows Vista® Ultimate 64-bit and employing eightfold paralleling.

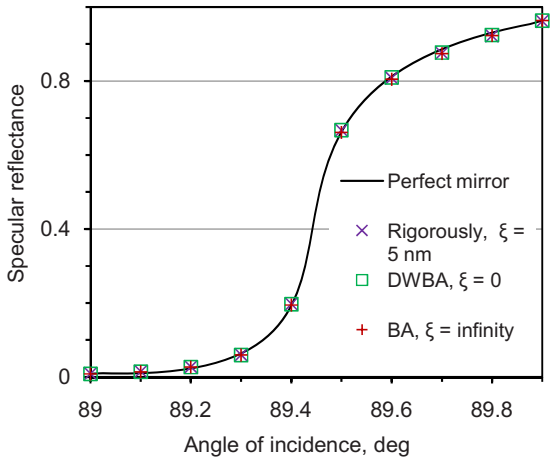

FIG. 4. (Color online) Specular TE reflectances of Au surfaces with $\sigma=0.15$ nm and at $\lambda=0.154$ nm plotted vs θ for different calculation models and ξ.

Figures 6 and 7 compare the approximate with rigorous models for $\lambda=0.154$ nm, $\sigma=1.5$ nm and different ξ. The reflectances calculated rigorously in the low-intensity domain in Fig. 6 for $\xi=10$ μm are approximately twice those obtained with the BA. For $\xi=0.1$ μm, the excess is already about fourfold. By contrast, close to the critical angle in Fig. 7 the rigorous data obtained for $\xi=0.1$ μm lie ~20% below the values calculated for this region with the DWBA. For $\xi=10$ μm, in the region of high intensities, the differences are still larger, to reach finally a few hundred percent. Such pronounced differences may give rise not only to overestimation of σ but to a wrong assessment of ξ as well, if they are deduced from a comparison of experimental with calculated data.[47] The behavior of the scattering intensity on ξ which is illustrated graphically in Fig. 7 matches qualitatively with the results obtained in the frame of the second-order DWBA

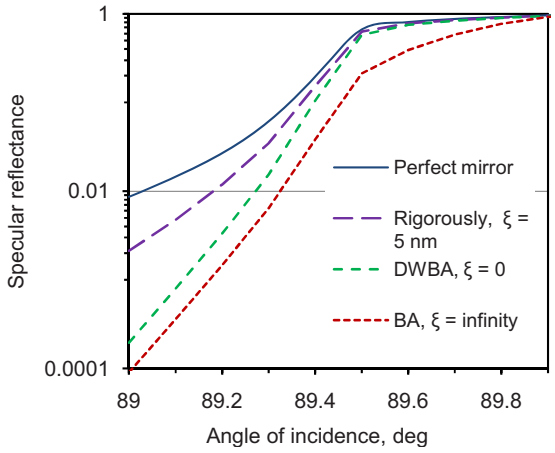

FIG. 5. (Color online) Same as in Fig. 4 but for $\sigma=1.5$ nm.

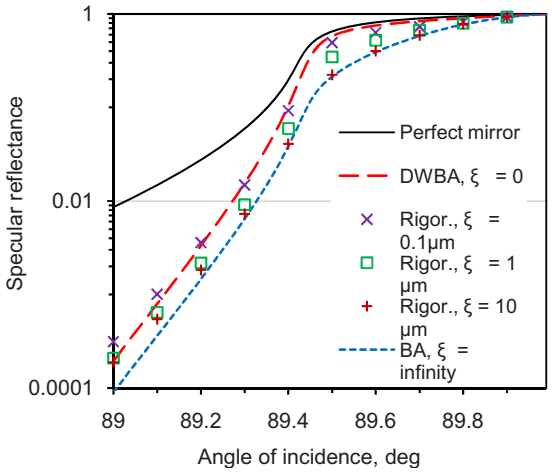

FIG. 6. (Color online) Specular TE reflectances of Au surfaces with $\sigma = 1.5$ nm and at $\lambda = 0.154$ nm plotted vs θ for different calculation models and ξ.

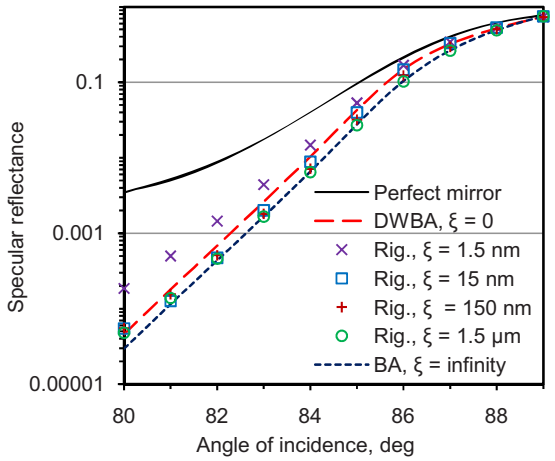

FIG. 8. (Color online) Specular TE reflectances of Au surfaces with $\sigma = 1.5$ nm and at $\lambda = 1.5$ nm plotted vs θ for different calculation models and ξ.

and the Rayleigh method,[48] while differing clearly in quantitative estimates, particularly for values of σ, ξ, and k^+ for which these and similar approximations do not work.[47–49]

To account for the fine structure of irregularities in the above example, one has to use ~100 asperities per d, several sample points per asperity, average over 9–25 random boundaries and assume 400–3200 collocation points. For $\xi = 10$ μm and $d = 1500$ μm, $\lambda/d \approx 1.E-7$, a value too small to be dealt with in any known rigorous numerical approach. For the MIM, however, this formidable scattering problem is found to be convergent and yields quite accurate results (the energy balance error is $\sim 1.E-6$) for $N = 400$ only and no speed-up techniques invoked. The time taken up by one computation on the above mentioned workstation is ~40 s.

Figures 8 and 9 plot graphs similar to those presented earlier but obtained for $\lambda = 1.5$ nm, $\sigma = 1.5$ nm and different ξ. For the minimum $\xi = 1.5$ nm, the rigorous results exceed by a few times those derived from the BA for large grazing angles, and are ~10% larger than the ones extracted from the DWBA close to the critical angle. For $\xi = 15$ nm, the differences are smaller, and as the correlation length continues to grow, rigorous calculations yield results which approach throughout the angular range covered the values derived from the BA, in full agreement with Ref. 48. In the examples with $\xi = 1.5$ nm, one has to take into account ~50 asperities per d, average over 9–25 random boundaries and use 200–2400 collocation points. None of the known convergence speed-up techniques was applied in this case too.

V. SUMMARY

The boundary integral equation method was considered for the smallest λ/d diffraction problems. To transform the diffraction problem for the quasiperiodic 2D Helmholtz equations in $\mathbb{R}^2$ to the single integral equation the boundary integral operators were used. A few distinctive features of the presented MIM and its implementation were pointed out. The special attention was focused on the main peculiarities of the MIM for $\lambda/d \ll 1$ as well as on a more general treatment of the energy conservation law applicable to absorption gratings and rough mirrors.

Calculations based on rigorous electromagnetic theory were performed using the MIM, which turned out to provide high accuracy and fast convergence for very large ratios of the characteristic period and height to wavelength. The developed MIM gives exact results and works fast in the x-ray

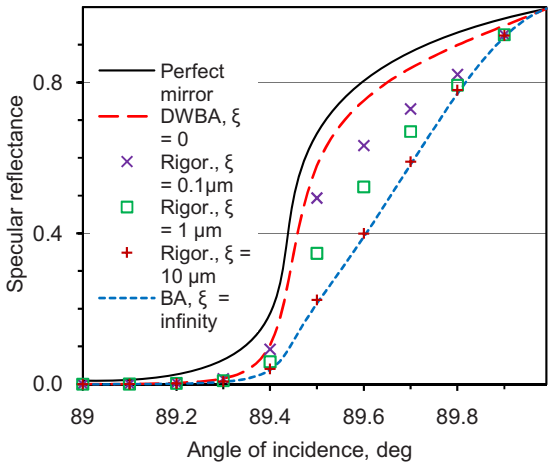

FIG. 7. (Color online) Same as in Fig. 6 but for linear y-scale.

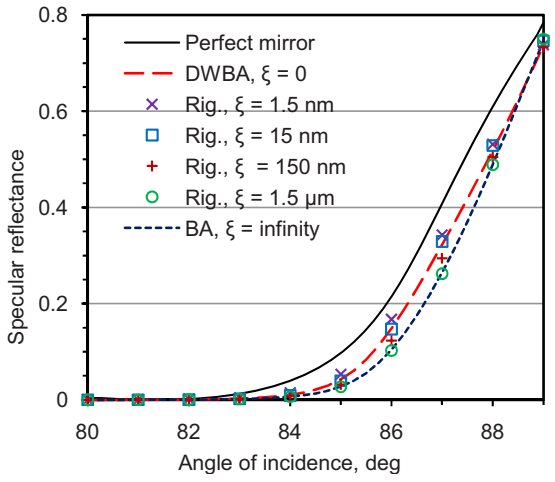

FIG. 9. (Color online) Same as in Fig. 8 but for linear y-scale.

range at grazing incidence, the most difficult case for any rigorous numerical code. Diffraction problems for bulk structures with arbitrary boundary profiles, including edges and random asperities, are treated using the MIM. Rigorous account of roughness with Gaussian surface statistics has been applied to x-ray specular reflectance of Au mirrors for different rms roughnesses, correlation lengths, and wavelengths.

The accurate results obtained by the rigorous method for intensities of x-ray scattering by rough mirrors may differ substantially from those derived using known asymptotics and approximate approaches. These differences may give rise, for instance, to wrong estimates of rms roughness and correlation length (slope angles) if they are determined by comparing experimental data with calculations. Besides, the rigorous approach permits taking into account any known roughness statistics. The proposed approach to numerical treatment of x-ray and neutron beam diffraction from rough surfaces permits one to determine accurately the specular and the diffuse components and can be extended to multilayer cases as well.[40,50]

ACKNOWLEDGMENTS

The author feels indebted to Andreas Rathsfeld (WIAS, Germany), Bernd Kleemann (Carl Zeiss AG, Germany), Gunther Schmidt (WIAS, Germany), and Sergey Sadov (New Foundland Memorial University, Canada) for fruitful discussions and information provided.

APPENDIX: DERIVATION OF THE ABSORPTION INTEGRAL

Because of the problem being invariant under translation by an integer number of periods along the axis perpendicular to the grooves, one may restrict oneself to an analysis of the heat power loss $\tilde{E}_A$ per grating period. $\tilde{E}_A$ can be calculated as the energy flux that has crossed the boundary Γ of the grating structure through an element of area bounded by the $x=0$, $x=d$, $z=0$, and $z=1$ planes:

$$\tilde{E}_A = \int_0^1 dz \int_\Gamma \mathbf{S}^- \mathbf{n} ds, \tag{A1}$$

where $\mathbf{S}^-$ is the time-averaged complex Poynting vector calculated at the boundary, $\mathbf{n}$ is the unit vector of the normal that is interior to the region under study, and arc length integration is performed along the cut of the boundary by the $z=0$ plane.

Recalling that $|\mathbf{S}^-|=0.5\ \mathrm{Re}\ \mathbf{E}^- \times \overline{\mathbf{H}^-}$ we open the vector and dot products for the TE and TM polarizations under the integral signs in Eq. (A1)

$$\tilde{E}_A^s = 0.5\ \mathrm{Re} \int_\Gamma [E_z^- (\overline{H_x^-} \cos b - \overline{H_y^-} \cos a) ds],$$

$$\tilde{E}_A^p = 0.5\ \mathrm{Re} \int_\Gamma \overline{H_z^-} (E_x^- \cos b - E_y^- \cos a) ds. \tag{A2}$$

As follows from Maxwell's equations

$$\partial_n \overline{E_z^-} = (-\overline{H_y^-} \cos a + \overline{H_x^-} \cos b)/\mathrm{i}\omega\mu^-,$$

$$\partial_n H_z^- = (-E_y^- \cos a + E_x^- \cos b)/\mathrm{i}\omega\epsilon^-. \tag{A3}$$

Substituting Eqs. (A2) and (A3), we obtain

$$\tilde{E}_A^s = 0.5\ \mathrm{Re} \int_\Gamma \frac{1}{\mathrm{i}\omega\mu^-} \partial_n \overline{E_z^-} E_z^- ds,$$

$$\tilde{E}_A^p = 0.5\ \mathrm{Re} \int_\Gamma \frac{1}{\mathrm{i}\omega\epsilon^-} \partial_n H_z^- \overline{H_z^-} ds. \tag{A4}$$

In studies of electromagnetic field losses at the grating, $\tilde{E}_A$, it should be normalized against the heat power losses of the incident wave E_A within a plane element of area bounded by the same planes $x=0$, $x=d$, $z=0$, and $z=1$:

$$E_A^s = 0.5\ \mathrm{Re} \int_0^d \frac{1}{\mathrm{i}\omega\mu^-} \partial_n \overline{E_z^i} E_z^i dx,$$

$$E_A^p = 0.5\ \mathrm{Re} \int_0^d \frac{1}{\mathrm{i}\omega\epsilon^-} \partial_n H_z^i \overline{H_z^i} dx. \tag{A5}$$

Substituting now the explicit form of the incident field of unit amplitude and of its normal derivative in Eq. (A5), recalling the boundary conditions, and taking account of simplifications in integration, we come to

$$E_A^s = 0.5\beta d/\omega\mu^+,$$

$$E_A^p = 0.5\beta d/\omega\epsilon^+. \tag{A6}$$

Using Eq. (A4) in conjunction with Eq. (A6), the normalized expressions for $\tilde{E}_A$, the electromagnetic field energy absorbed in the grating, transform to

$$A^s = \frac{\tilde{E}_A^s}{E_A^s} = \frac{1}{\beta d} \mathrm{Re} \int_\Gamma \frac{\mathrm{i}\mu^+}{\mu^-} \partial_n \overline{E_z^-} E_z^- ds,$$

$$A^p = \frac{\tilde{E}_A^p}{E_A^p} = \frac{1}{\beta d} \mathrm{Re} \int_\Gamma \frac{\mathrm{i}\epsilon^+}{\epsilon^-} \partial_n H_z^- \overline{H_z^-} ds. \tag{A7}$$

Recalling that $\mathrm{Re}\ O = \mathrm{Im}\ \mathrm{i}O$, Eq. (A7) can be recast using the universal field component u^+ and its normal derivative v^+

$$A = \frac{1}{\beta d} \mathrm{Im} \int_\Gamma u^+ \overline{v^+} ds. \tag{A8}$$

Equation (A8) for the absorption A of an electromagnetic field by a grating in classical diffraction is a particular case of the expression presented in Ref. 29 for conical diffraction and derived by applying the second Green's identity to boundary functions and performing the integration by parts.

[1] A. Caticha, Phys. Rev. B **62**, 3639 (2000).
[2] S. Dietrich and A. Haase, Phys. Rep. **260**, 1 (1995).
[3] K. F. Warnick and W. C. Chew, Waves Random Media **11**, R1 (2001).
[4] *Light Scattering and Nanoscale Surface Roughness*, edited by A. A. Maradudin (Springer, New York, 2007).
[5] N. Déchamps, N. Beaucoudrey, C. Bourlier, and S. Toutain, J. Opt. Soc. Am. A **23**, 359 (2006).
[6] M. Saillard and A. Sentenac, Waves Random Media **11**, R103 (2001).
[7] M. V. Babich and V. S. Buldyrev, *Asymptotic Methods in Short-Wavelength Diffraction Theory* (Alpha Science, Oxford, 2007).
[8] U. Pietsch, V. Holy, and T. Baumbach, *High-Resolution X-Ray Scattering:*

From Thin Films to Lateral Nanostructures (Springer-Verlag, Heidelberg, 2004).
[9]T. M. Elfouhaily and C.-A. Guerin, Waves Random Media **14**, R1 (2004).
[10]A. V. Andreev, Phys. Lett. A **219**, 349 (1996).
[11]M. Saillard, D. Maystre, and J. P. Rossi, Opt. Acta **33**, 1193 (1986).
[12]A. Rathsfeld, G. Schmidt, and B. H. Kleemann, Comm. Comp. Phys. **1**, 984 (2006).
[13]B. H. Kleemann and J. Erxmeyer, J. Mod. Opt. **51**, 2093 (2004).
[14]M. Neviere and E. Popov, *Light Propagation in Periodic Media: Differential Theory and Design* (Marcel Dekker, New York, 2002).
[15]E. Popov, B. Bozhkov, D. Maystre, and J. Hoose, Appl. Opt. **38**, 47 (1999).
[16]B. H. Kleemann, J. Gatzke, Ch. Jung, and B. Nelles, Proc. SPIE **3150**, 137 (1997).
[17]M. Saillard and D. Maystre, J. Opt. Soc. Am. A **7**, 982 (1990).
[18]*Electromagnetic Theory of Gratings*, edited by R. Petit (Springer, Berlin, 1980).
[19]L. I. Goray, J. F. Seely, and S. Yu. Sadov, J. Appl. Phys. **100**, 094901 (2006).
[20]L. I. Goray and S. Y. Sadov, in *Diffractive Optics and Micro-Optics*, OSA Trends in Optics and Photonics Series Vol. 75, edited by R. Magnusson (Optical Society of America, Washington, DC, 2002), p. 365.
[21]L. I. Goray, Proc. SPIE **4291**, 1 (2001).
[22]L. I. Goray, I. G. Kuznetsov, S. Y. Sadov, and D. A. Content, J. Opt. Soc. Am. A **23**, 155 (2006).
[23]L. I. Goray, Nucl. Instrum. Methods Phys. Res. A **536**, 211 (2005).
[24]J. F. Seely, L. I. Goray, B. Kjornrattanawanich, J. M. Laming, G. E. Holland, K. A. Flanagan, R. K. Heilmann, C.-H. Chang, M. L. Schattenburg, and A. P. Rasmussen, Appl. Opt. **45**, 1680 (2006).
[25]C.-H. Chang, J. C. Montoya, M. Akilian, A. Lapsa, R. K. Heilmann, M. L. Schattenburgand, M. Li, K. A. Flanagan, A. P. Rasmussen, J. F. Seely, J. M. Laming, B. Kjornrattanawanich, and L. I. Goray, J. Vac. Sci. Technol. B **22**, 3260 (2004).
[26]L. I. Goray and J. F. Seely, Appl. Opt. **41**, 1434 (2002).
[27]*Modern Analysis of Scattering Phenomena*, edited by D. Maystre and J. C. Dainty (Hilger, New York, 1991).
[28]*Scattering in Volumes and Surfaces*, edited by M. Nieto-Vesperinas and J. C. Dainty (Elsevier, North-Holland, 1990).
[29]L. I. Goray and G. Schmidt, J. Opt. Soc. Am. A **27**, 585 (2010).
[30]B. Kleemann, A. Mitreiter, and F. Wyrowski, J. Mod. Opt. **43**, 1323 (1996).
[31]A. Pomp, J. Mod. Opt. **38**, 109 (1991).
[32]D. Colton and R. Kress, *Integral Equation Methods in Scattering Theory* (Springer, Berlin, 1984).
[33]L. Tsang, J. A. Kong, K.-H. Ding, and C. O. Ao, *Scattering of Electromagnetics Waves: Numerical Simulations* (Wiley, New York, 2001).
[34]C. M. Linton, J. Eng. Math. **33**, 377 (1998).
[35]S. Y. Sadov, in *Advances in Difference Equations*, edited by I. Gyori, G. Ladas, and S. Elaydi (Gordon and Breach, Amsterdam, 1997), p. 551.
[36]L. I. Goray and G. M. Savitzky, *All-Union Seminar Questions of Applied Holography* (The Academy of Sciences, Tbilisi, USSR, 1989), p. 20 (in Russian).
[37]The Center for X-Ray Optics, X-ray Interactions With Matter, Available from: http://henke.lbl.gov/
[38]*Handbook of Mathematical Functions, 10th Printing*, edited by M. Abramowitz and I. Stegun (National Bureau of Standards, Washington, DC, 1972).
[39]S. K. Sinha, E. B. Sirota, S. Garoff, and H. B. Stanley, Phys. Rev. B **38**, 2297 (1988).
[40]Website at http://www.pcgrate.com
[41]L. I. Goray, Proc. SPIE **6617**, 661719 (2007).
[42]L. I. Goray, Proc. SPIE **7390**, 73900V (2009).
[43]L. I. Goray, N. I. Chkhalo, and G. E. Tsyrlin, Tech. Phys. **54**, 561 (2009).
[44]L. I. Goray, N. I. Chkhalo, and Y. A. Vainer, Tech. Phys. Lett. **36**, 108 (2010).
[45]E. Spiller, *Soft X-Ray Optics* (SPIE, Bellingham, 1994).
[46]L. Névot and P. Croce, Rev. Phys. Appl. **15**, 761 (1980).
[47]I. D. Feranchuk, S. I. Feranchuk, and A. P. Ulyanenkov, Phys. Rev. B **75**, 085414 (2007).
[48]D. K. G. de Boer, Phys. Rev. B **49**, 5817 (1994); **51**, 5297 (1995); **53**, 6048 (1996).
[49]T. A. Leskova and A. A. Maradudin, Waves Random Media **7**, 395 (1997); **9**, 461 (1999).
[50]L. I. Goray, "Application of the boundary integral equation method to very small wavelength-to-period diffraction problems," Waves Random Media (to be published).